Journal of Power Sources 268 (2014) 331–340

Contents lists available at ScienceDirect

Journal of Power Sources

journal homepage: www.elsevier.com/locate/jpowsour

A series of copper-free ternary oxide catalysts $ZnAlCe_x$ used for hydrogen production via dimethyl ether steam reforming

Lijie Zhang [a], Ming Meng [a, *], Xiaojing Wang [a, *], Shuang Zhou [a], Lijuan Yang [a], Tianyong Zhang [a], Lirong Zheng [b], Jing Zhang [b], Tiandou Hu [b]

[a] Collaborative Innovation Center for Chemical Science & Engineering, Tianjin Key Laboratory of Applied Catalysis Science and Engineering, School of Chemical Engineering and Technology, Tianjin University, Tianjin 300072, PR China
[b] Beijing Synchrotron Radiation Facility, Institute of High Energy Physics, Chinese Academy of Sciences, Beijing 100049, PR China

HIGHLIGHTS

- Ce-substitution greatly improves the DME SR performance of $ZnAlCe_x$ catalysts.
- The optimized CeO_2 content in $ZnAlCe_x$ catalysts is 20% by weight.
- The presence of Ce in $ZnAlCe_x$ can enhance H_2 desorption at lower temperature.
- $ZnAlCe_x$ catalysts exhibit much lower CO selectivity than Cu-based one.
- The catalyst $ZnAlCe_{0.2}$ shows very high catalytic stability even at 420 °C.

ARTICLE INFO

Article history:
Received 2 April 2014
Received in revised form
8 June 2014
Accepted 9 June 2014
Available online 18 June 2014

Keywords:
Dimethyl ether
Steam reforming
Hydrogen production
Zinc-based catalyst

ABSTRACT

Ce-substituted ternary oxide catalysts $ZnAlCe_x$ were prepared and employed in dimethyl ether steam reforming (DME SR) to produce hydrogen. XRD, XAFS (XANES & EXAFS), H_2O-TPD, CH_3OH-TPD and TPSR techniques were used for catalyst characterization. It is found that the catalytic performance of these catalysts is dependent on Ce content. The catalyst containing 20 wt% CeO_2 exhibits the best catalytic performance. Its calculated TOF (0.034 s^{-1}) is nearly three times to that of ZnAlO. The kinetic results reveal that the addition of 20 wt% CeO_2 to $ZnAlCe_x$ greatly decreases the apparent activation energy (Ea) of DME SR, due to the formation of new reaction sites such as Ce^{4+}–O–Zn^{2+} linkages. XRD and EXAFS analyses indicate that Ce addition can not only decrease the crystallite size of ZnO and $ZnAl_2O_4$, but also tune the relative contents of them. The results of H_2O-TPD and CH_3OH-TPD show that Ce addition can lower H_2 desorption temperature, which accounts well for the better catalytic performance of $ZnAlCe_x$. It is worth noting that the Zn-based catalysts display much lower CO selectivity than the Cu-based one, especially the Ce-substituted $ZnAlCe_x$. Start-off durability tests demonstrate that this series of catalysts also possess high catalytic stability.

1. Introduction

Fuel cells, which exhibit lots of merits such as high energy efficiency and low pollution, have been regarded as an environment-friendly energy [1,2]. However, how to supply H_2 to the fuel cells is still a remaining problem. Employment of tanks with ready-made high pressure H_2 seems feasible, but it will greatly increase the cost and the danger induced by H_2 leak. To solve this problem, onboard supply of H_2 is proposed via catalytic reforming routes using H_2-containing materials as reactants, such as alkanes, alcohols and ethers [3–5].

The efficiency for hydrogen production onboard from reforming processes is crucial to the application and commercialization of hydrogen-based fuel cells. Steam reforming (SR) has been proved to be a potential route for H_2 production due to its high H_2 yield and good product quality. By now, many kinds of H_2-containing raw materials have been employed for hydrogen production through SR routes, such as ethanol, methanol and DME. Among them, ethanol SR needs relatively high temperature and may produce CH_4 or coke. Methanol SR (MSR) can operate at lower temperature, giving high-quality products; however, the toxicity of methanol limits its application. Compared with methanol or ethanol, DME is a better

* Corresponding authors. Tel./fax: +86 (0)22 2789 2275.
E-mail address: mengm@tju.edu.cn (M. Meng).

http://dx.doi.org/10.1016/j.jpowsour.2014.06.045
0378-7753/

candidate for hydrogen production via SR process since it has higher H/C ratio and no toxicity. In addition, DME molecule has no C–C bond, which can greatly inhibit the formation of coke during DME reforming [6].

DME SR contains two successive reactions including DME hydrolysis to methanol and the subsequent methanol SR (MSR) to H_2 and CO_2 [7]. An important side reaction is the reverse water gas shift reaction (r-WGS), which takes place over MSR catalysts [8]. Some other side reactions, such as decomposition of DME and methanol, may also occur during DME SR process [8], as shown below.

DME SR

$$(CH_3)_2O + 3H_2O \rightarrow 6H_2 + 2CO_2 \quad \Delta H^{\Theta} = 135 \text{ kJ mol}^{-1} \tag{1}$$

DME hydrolysis

$$(CH_3)_2O + H_2O \rightarrow 2CH_3OH \quad \Delta H^{\Theta} = 37 \text{ kJ mol}^{-1} \tag{2}$$

Methanol SR

$$CH_3OH + H_2O \rightarrow 3H_2 + CO_2 \quad \Delta H^{\Theta} = 49 \text{ kJ mol}^{-1} \tag{3}$$

r-WGS

$$CO_2 + H_2 \rightarrow CO + H_2O \quad \Delta H^{\Theta} = 41 \text{ kJ mol}^{-1} \tag{4}$$

DME decomposition

$$CH_3OCH_3 \rightarrow CH_4 + CO + H_2 \quad \Delta H^{\Theta} = -1 \text{ kJ mol}^{-1} \tag{5}$$

Methanol decomposition

$$CH_3OH \rightarrow 2H_2 + CO \quad \Delta H^{\Theta} = 91 \text{ kJ mol}^{-1} \tag{6}$$

Solid acids, especially heteropoly acid, zeolite and alumina, are often used for the hydrolysis of DME to methanol [9–11], while metallic catalysts such as Cu-based ones [7,12,13] or Zn-based ones [14–16] are employed for MSR. Although Cu-containing catalysts are highly active for MSR, they exhibit low thermal stability and unsatisfactory durability due to the easy agglomeration of copper species at high temperature. So, in recent years copper-free catalysts are getting more and more attention. It has been reported that Zn-based catalysts possess high CO_2-selectivity and high catalytic stability in MSR reaction [14,15] and DME SR reaction [16]. However, compared with Cu-based catalysts, Zn-based catalysts usually run at relatively high temperature. In order to simultaneously increase the catalytic activity and decrease the reaction temperature, further modification of Zn-based catalysts is necessary. Since CeO_2 possesses good redox property, high oxygen storage capacity and strong interaction with other components [17], in this work it was selected to partially substitute the Al in ZnO–Al_2O_3 oxides to prepare the ternary oxide catalysts $ZnAlCe_x$. It is shown that this series of catalysts display remarkably improved catalytic performance for DME SR, especially the very low selectivity to CO. Several techniques were employed to characterize these catalysts, such as XRD, XANES, EXAFS, H_2O-TPD, CH_3OH-TPD and TPSR. Based upon the results of activity and multiple characterizations, the effect of CeO_2 substitution on the catalytic performance and catalyst structures was revealed.

2. Experimental

2.1. Catalyst preparation

Co-precipitation method was used for the preparation of ZnAlCeO oxides. Firstly, according to the contents of Zn, Al and Ce in the catalysts, a mixed solution of metal nitrates was prepared. Then, the mixed solution and aqueous ammonia were added dropwise into a stirred flask containing 100 mL deionized water. The pH was kept around 7.5 during the precipitation process. The precipitate was aged in the mother liquid at 70 °C for 2 h, and subsequently washed with 70 °C deionized water for 3 times. After drying at 120 °C overnight, the precipitate was calcinated at 500 °C for 4 h to form the ternary oxides $ZnAlCe_x$ (x = 0, 0.05, 0.1, 0.2 or 0.3, x represents the content of CeO_2 by weight). In these oxides, the content of ZnO and the total content of CeO_2 and Al_2O_3 were fixed at 40 wt% and 60 wt%, respectively. Before use, a mixture of $ZnAlCe_x$ and γ-Al_2O_3 with the weight ratio of 3:1 was mixed, pressed, crushed and sieved to 40–60 mesh.

2.2. Catalytic activity and stability measurements

The catalytic performance evaluation of the $ZnAlCe_x$ for DME SR was conducted in a conventional quartz tube reactor under atmospheric pressure. Each time, 500 mg sample was used. The mixed stream of 40 mL min^{-1} N_2, 50 mL min^{-1} H_2O (g) and 10 mL min^{-1} DME was purveyed to the catalyst bed. The analysis of reactants and products was performed using an Agilent 7890A gas chromatograph. The DME conversion, H_2 yield and C1 selectivity are used to evaluate the performance of these catalysts as described elsewhere [8,18]. The stability of the catalyst was evaluated by using a continuous start-off test, in which 14 h cyclic heating to 420 °C and cooling to RT in the DME SR feed stream was performed on the catalyst to observe the alteration of DME conversion.

2.3. Catalyst characterization

A Quantachrome QuadraSorb SI instrument was used to measure the N_2 adsorption–desorption isotherms at 77 K. The samples were evacuated at 300 °C for 6 h to remove the physisorbed substances. The BET method was used to calculate the specific surface area (S_{BET}). Pore volume and average pore diameter of the samples were calculated by using BJH method.

The crystalline phase of the samples was determined by X-ray diffraction (XRD) on a D8 diffractometer (Bruker Company) using Cu Kα as radiation source (λ = 0.15418 nm). The patterns were collected at 40 kV and 40 mA. The 2θ scanning range is 20–90° with a stepsize of 0.02°.

CH_3OH pulse adsorption, the temperature-programmed desorption of H_2O (H_2O-TPD) or CH_3OH (CH_3OH-TPD) as well as the temperature-programmed surface reaction (TPSR) were all conducted on the TP-5079 instrument equipped with a mass spectrometry (Hiden HPR20). The procedures are similar to those in literature [19]. For H_2O-TPD experiments, 50 mg powder sample was first loaded into the quartz tube reactor and then heated to 400 °C for half an hour pretreatment in helium (50 mL min^{-1}) so as to ensure a clean surface. After the catalyst bed cooled to 100 °C, pulses of deionized water (1.0 μL) (repeated 5 times with 1 min interval) were purveyed into the catalyst bed. To removal the gaseous water in reaction system, the sample cell was flushed with pure helium for another hour at 100 °C. Subsequently, the sample

cell was heated to 600 °C (10 °C min^{-1}) for water desorption. During CH_3OH pulse adsorption and CH_3OH-TPD, the catalyst (50 mg) pretreatment is the same as that for H_2O-TPD. After the catalyst bed cooled to ambient temperature, pulses of CH_3OH (1.0 μL) were injected into the catalyst bed repeatedly (30-min interval between each injection) until the signal of mass spectrometry for CH_3OH was not changed any more. Finally, the sample was heated to 700 °C (10 °C min^{-1}) for MeOH desorption. In TPSR experiments, the catalyst (50 mg) was first pretreated at 400 °C for 30 min, after the temperature was decreased to 100 °C, the pulse adsorption of deionized water (5 μL) was carried out; to remove the physisorbed and gaseous H_2O, the catalyst bed was flushed with pure helium for 1 h; in the next, methanol (5 μL) was also injected for adsorption, after a similar helium flushing for 30 min, the sample was heated to 700 °C (10 °C min^{-1}). No HCHO was detected during this period.

X-ray absorption near-edge structure (XANES) and extended X-ray absorption fine structure (EXAFS) of the catalysts were measured on the XAFS station in the 1W1B beamline of Beijing Synchrotron Radiation Facility (BSRF) using a Si(111) double-crystal as monochromator. The Zn *K*-edge spectra of $ZnAlCe_x$, ZnO and $ZnAl_2O_4$ were collected at an average ring current of 200 mA in transmission mode. During measurements, zinc foil was used to calibrate the energy. The obtained spectra were back-subtracted and converted to *k* space. Then the Fourier transforming was performed on the k^3-weighted EXAFS data (k = 3–13 $Å^{-1}$) using a Hanning window function to get the radial structure functions (RSFs).

3. Results

3.1. Catalytic performance

3.1.1. DME SR

The catalytic performance of the catalysts for DME SR is shown in Fig. 1. The content of Ce has a significant influence on the catalytic activity. The catalyst $ZnAlCe_{0.2}$ exhibits the best activity for DME conversion. At 400 °C, the DME conversion over $ZnAlCe_{0.2}$ is 90.1%, much higher than that of the catalyst without Ce. Arrhenius plots for DME SR over $ZnAlCe_0$ and $ZnAlCe_{0.2}$ are acquired from the rates of DME consumption over 50 mg $ZnAlCe_x$ catalysts between 360 °C and 440 °C, which are displayed in Fig. 2. Rather good linearity is observed; from the slope of lines, apparent activation energies (E_a) were determined, as shown in Table 1. It is observed that doping of 20 wt% CeO_2 into $ZnAlCe_x$ catalyst induces a substantial decrease in Ea (11.4 kJ mol^{-1} difference), which is in good agreement with the enhanced catalytic activity. Assuming that the MeOH chemisorption sites (estimated from the CH_3OH pulse adsorption) were the active site for DME SR, the turnover frequencies (TOF) of the catalysts were calculated. As seen in Table 1, with the increase of Ce content from 0 to 20 wt%, the TOF increases from 0.013 to 0.034 s^{-1}, indicating an obvious enhancement effect of Ce on DME SR. However, as the Ce amount increases from 20 to 30 wt%, DME conversion decreases, which is consistent with the increased Ea (from 184.1 to 186.2 kJ mol^{-1}). The H_2 yield versus reaction temperature is shown in Fig. 3. It is found that the effect of Ce addition on H_2 yield is similar to that on DME conversion; the catalyst containing 20 wt% CeO_2 gives the highest H_2 yield. During DME SR reaction, C1 species in the effluent gas were also monitored. No methanol was found above 350 °C, suggesting that the hydrolysis of DME to methanol may be the rate-determining step (RDS) for the whole DME SR reaction. Since the CH_4 selectivity (<1%) is always very low and neglectable, CO_2 and CO are regarded as the main C1 products during reaction. The correlation between CO selectivity and reaction temperature is depicted in Fig. 4. Our previous work on Cu catalysts [18] has shown that Cu-based catalysts always exhibit high CO selectivity (~20%) when DME reaches full conversion, but on $ZnAlCe_0$ catalyst it is only ~9%. After Ce addition, CO selectivity is further lowered, probably due to the improved oxidation performance of the catalysts containing Ce.

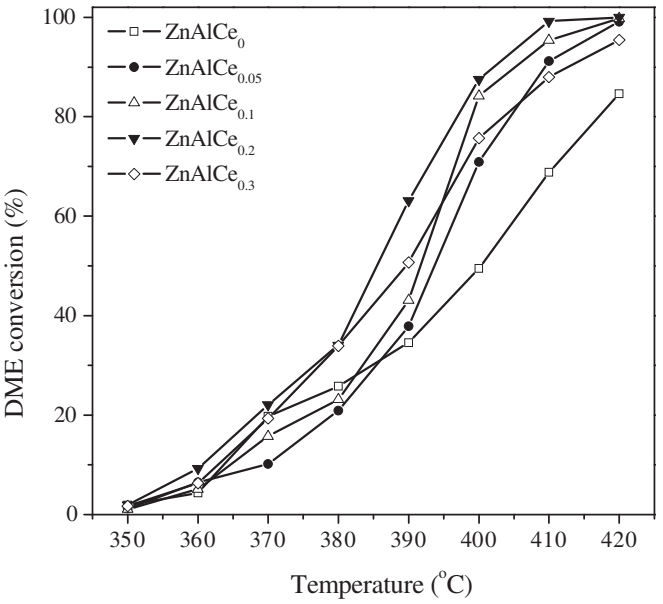

Fig. 1. DME conversion determined at different temperatures over the $ZnAlCe_x$ catalysts.

3.1.2. DME decomposition

To further investigate the function of Ce addition, DME decomposition over $ZnAlCe_x$ in the absence of water was conducted, the results of which are shown in Fig. 5. According to Eq. (5), DME decomposition reaction can generate the byproducts CH_4 and CO, which are not expected. From Fig. 5, it is observed that the order of DME conversion in DME decomposition reaction for different catalysts is different from that in DME SR. As the content of CeO_2 increases, the DME decomposition activity decreases

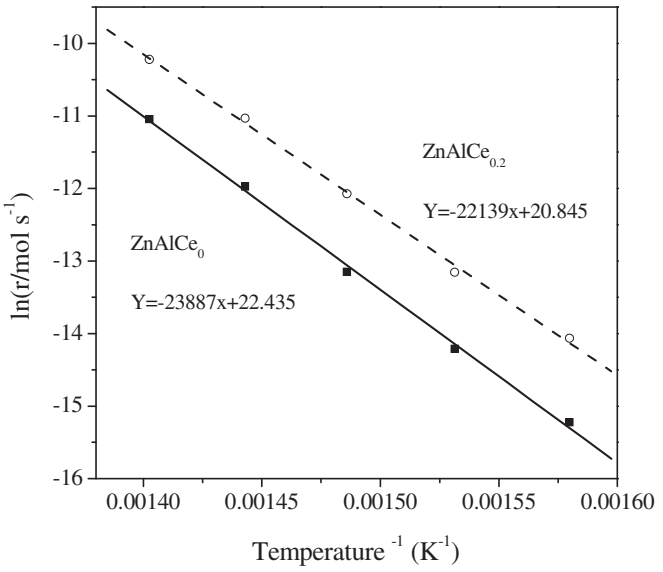

Fig. 2. Arrhenius plots for DME SR reaction over the $ZnAlCe_0$ and $ZnAlCe_{0.1}$ catalysts (catalyst weight: 50 mg, GHSV: 12,000 mL h^{-1} g_{cat}^{-1}, 10% DME, 50% H_2O and 40% N_2).

Table 1
Specific surface (SSA), pore volume (PV), relative amounts of adsorbed CH_3OH (ADM), apparent activation energy and TOF of $ZnAlCe_x$ catalysts.

Catalyst	SSA ($m^2\ g^{-1}$)	PV ($mL\ g^{-1}$)	PD (nm)	E_a ($kJ\ mol^{-1}$)[a]	ADM ($mmol\ g^{-1}$)[b]	TOF (s^{-1})[c]
$ZnAlCe_0$	158	0.18	4.6	195.5	0.240	0.013
$ZnAlCe_{0.05}$	137	0.19	5.6	192.7	0.258	0.022
$ZnAlCe_{0.1}$	122	0.22	6.7	192.8	0.260	0.028
$ZnAlCe_{0.2}$	111	0.21	7.4	184.1	0.259	0.034
$ZnAlCe_{0.3}$	80	0.15	7.5	186.2	0.178	0.035

[a] Apparent activation energy (E_a) was estimated from Arrhenius equation based on the activity over all the catalysts (50 mg) at 1 atm total pressure (10% DME, 50% H_2O and 40% N_2).
[b] Methanol adsorption amount was calculated from the area of the peaks in the CH_3OH pulse adsorption profiles.
[c] Turnover frequency (TOF) was estimated based on the ADM results and the activity tests over all the catalysts (50 mg) at 400 °C and 1 atm total pressure (10% DME, 50% H_2O and 40% N_2).

dramatically. The DME conversion during its decomposition over $ZnAlCe_0$ is as high as 21.4% at 400 °C, while it is only 3.2% over $ZnAlCe_{0.3}$ at the same temperature. Generally, Al^{3+} in the ZnAlO catalysts is responsible for DME decomposition reaction [16]. Thus, the gradually decreased DME conversion may be attributed to the decreased content of Al_2O_3. During DME SR the very low CH_4 selectivity (<1%) suggests that the decomposition of DME is neglectable, and that the existence of water may have restrained the DME decomposition.

3.2. Catalyst characterization

3.2.1. Texture and XRD characterization

The S_{BET} and pore volume of $ZnAlCe_x$ samples are listed in Table 1. It is found that the partial substitution of Al by Ce decreases the S_{BET}. The surface area of $ZnAlCe_0$ is 158 $m^2\ g^{-1}$, while it is only 80 $m^2\ g^{-1}$ for $ZnAlCe_{0.3}$. It is known that Al_2O_3 often possesses much higher surface area than CeO_2; so, the gradually decreased surface area may be due to the reduction of Al_2O_3 content. The XRD patterns displayed in Fig. 6 indicate that all the $ZnAlCe_x$ samples exhibit a group of diffraction peaks at 36.3, 31.8, 34.4 and 62.9°,

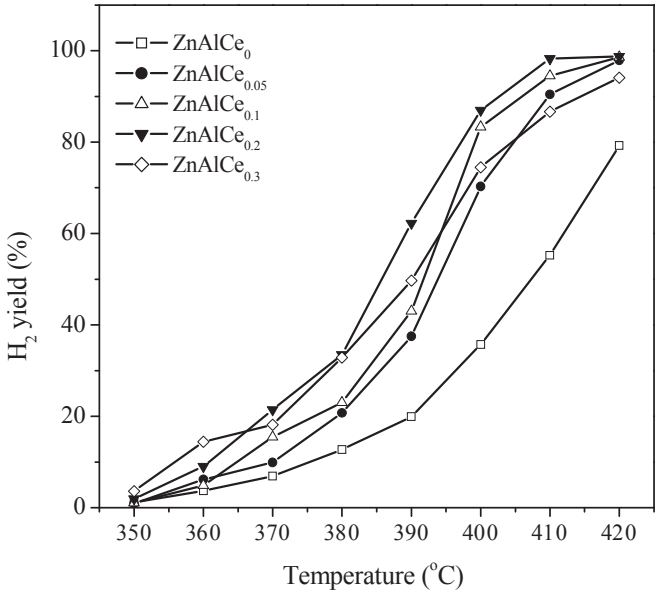

Fig. 3. H_2 yield determined at different temperatures over the $ZnAlCe_x$ catalysts during DME SR.

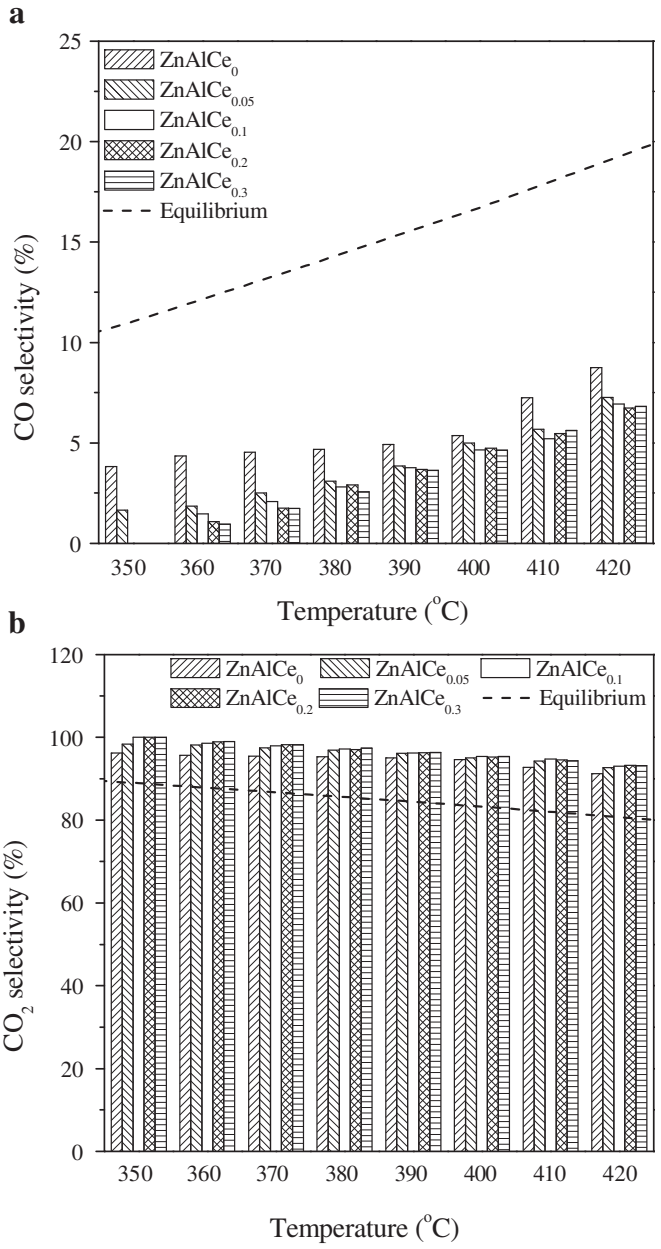

Fig. 4. CO selectivity (a) and CO_2 selectivity (b) versus reaction temperature over $ZnAlCe_x$ catalysts.

meaning the presence of zincite phase. The $ZnAl_2O_4$ phase is also observed for all the catalysts. Ce species in the $ZnAlCe_x$ mainly exist as cubic CeO_2 phase. With the increase of Ce content the diffraction peaks for both $ZnAl_2O_4$ and ZnO gradually decreases; the former may be caused by the reduction of Al_2O_3 content, while the later may be due to the decline of ZnO crystallite size.

3.2.2. Zn K-edge XANES and RSFs

In order to reveal the micro-structures of Zn species in the catalysts, Zn *K*-edge XANES and EXAFS characterizations were conducted. Fig. 7(a) shows the XANES spectra of ZnO, $ZnAl_2O_4$ and $ZnAlCe_x$ samples. As reported in literature [20], the spectrum of pure ZnO exhibits a 1s → 4p absorption peak at about 9667 eV, while that of $ZnAl_2O_4$ shows the peaks at about 9663 and 9671 eV. For $ZnAlCe_x$ catalysts, all of the three peaks are observed,

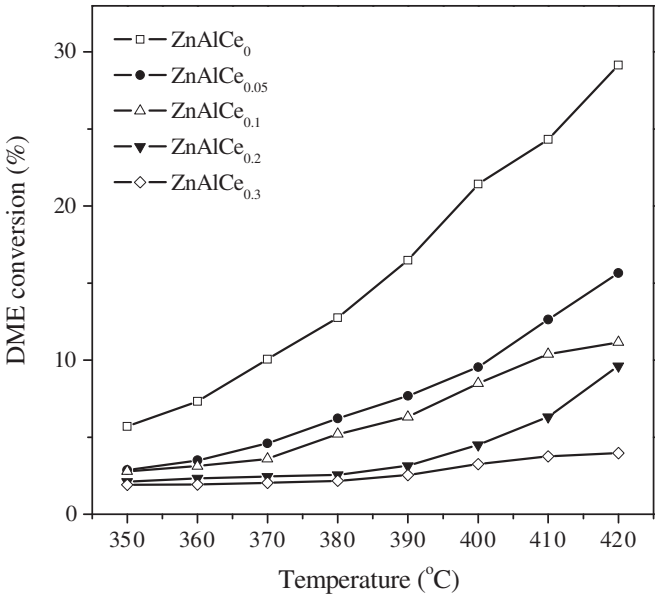

Fig. 5. DME decomposition conversion determined at different temperatures over the $ZnAlCe_x$ catalysts.

suggesting the co-existence of ZnO and $ZnAl_2O_4$ in the catalysts, which is supported by the XRD results. With the increase of Ce content, the peaks centered at 9663 and 9671 eV get weaker while the peak at about 9667 eV turns stronger, which implies that the content of ZnO increases, while that of $ZnAl_2O_4$ decreases.

The RSFs of the catalysts derived from Zn *K*-edge EXAFS data are shown in Fig. 7(b). The peaks at 0.154 and 0.289 nm for ZnO are attributed to Zn–O and Zn–Zn coordination shells, while those for $ZnAl_2O_4$ appear at 0.154 nm (Zn–O) and 0.305 nm (Zn–Al/Zn–Zn), respectively. For the catalysts $ZnAlCe_x$, the first peak (Zn–O) also appears at the same position, but the second one (0.298 nm) is observed between 0.289 and 0.305 nm, which suggests that the Zn in these catalysts should exist in a mixture state of ZnO and

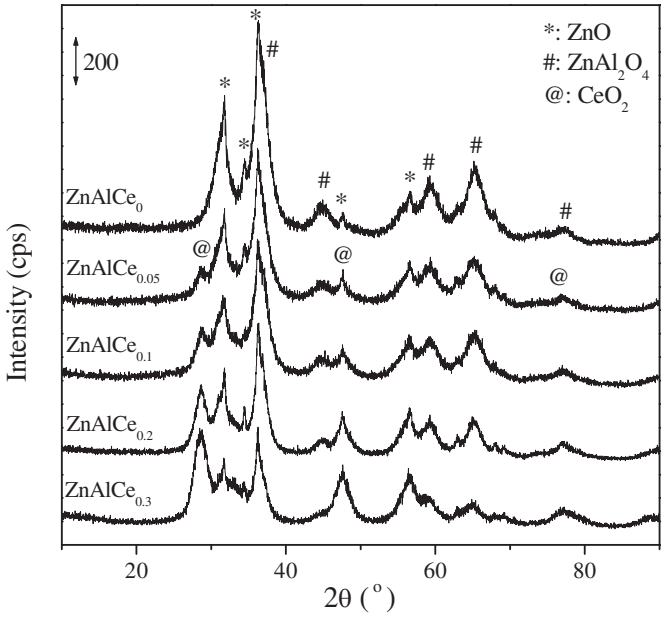

Fig. 6. XRD patterns of the $ZnAlCe_x$ catalysts.

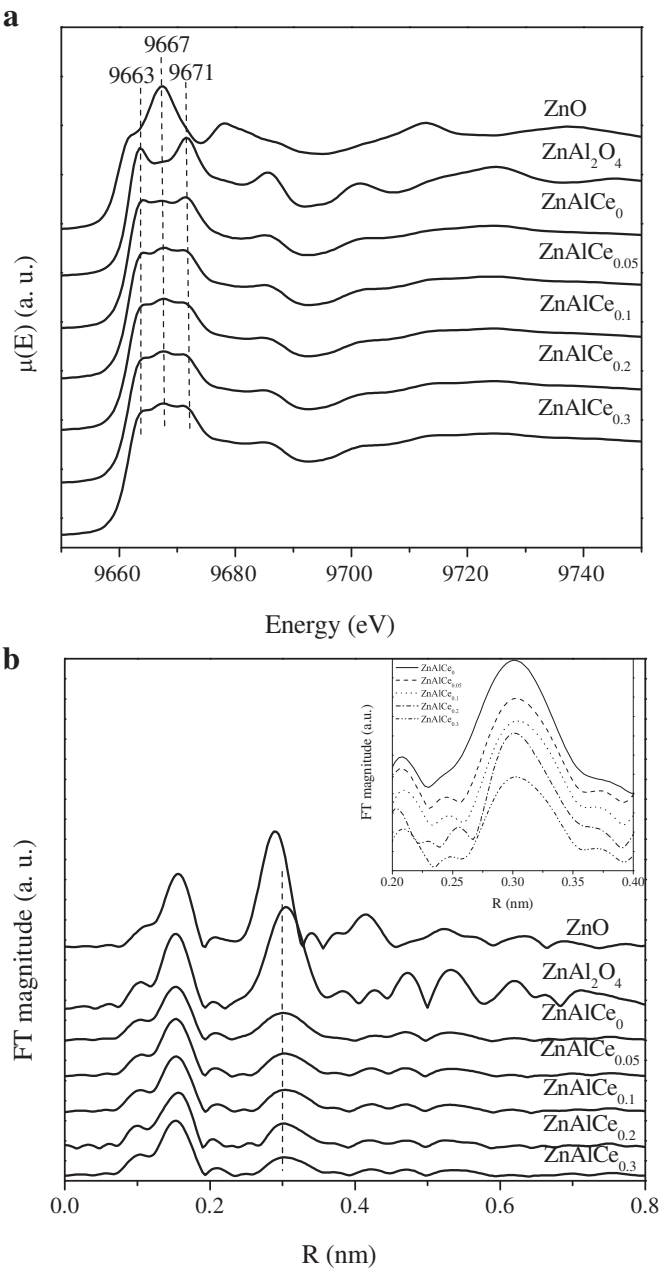

Fig. 7. XANES spectra (a) and radial structure functions (RSFs) (b) derived from Zn *K*-edge EXAFS spectra of the $ZnAlCe_x$ catalysts and reference compounds.

$ZnAl_2O_4$, as demonstrated by XRD and EXAFS results. However, compared with the reference compounds, the catalysts $ZnAlCe_x$ exhibit much weaker amplitude for the second coordination peaks, implying the much smaller crystallite size of Zn species in the catalysts. Additionally, by careful observation it can still be found that the Ce-containing catalysts also exhibit a little weaker amplitude for the second coordination peaks than $ZnAlCe_0$ without Ce (see the inset in Fig. 7(b)). This result further demonstrates that the introduction of Ce to ZnAlO catalysts can effectively decrease the crystallite size of ZnO and $ZnAl_2O_4$ phases.

3.2.3. H_2O-TPD

The TPD spectra of the catalysts after water adsorption are presented in Fig. 8(a). It is reported that water often adsorbs dissociatively on oxide surface, forming surface hydroxyl groups

[21,22], as described in Eq. (7), where A site represents the metal ion, while B site stands for the oxygen ion. In the catalysts $ZnAlCe_x$, surface Zn^{2+} ions and lattice oxygen ions may serve as site A and site B, respectively. Two desorption peaks are detected for all the catalysts. The first peak (~210 °C) could be assigned to the desorption of adsorbed H_2O in molecular state, while the second peak appearing at high temperature (above 470 °C) may correspond to the desorption of the water produced from the interaction of surface −OH groups. As the content of Ce increases, both of the two desorption peaks decrease, meaning that the doping of Ce inhibits H_2O adsorption to some extent, probably due to the decreased S_{BET} of $ZnAlCe_x$ catalysts. However, the presence of Ce seems favorable to H_2 desorption. From the H_2O-TPD profiles shown in Fig. 8(b), it is seen that the Ce-containing catalysts exhibit lower H_2 desorption temperature. On the surface of oxides, the hydrogen desorption often takes place via the interaction of surface hydroxyl groups, as illustrated in Eq. (8) [23]. The addition of Ce may facilitate the decomposition of surface −OH species.

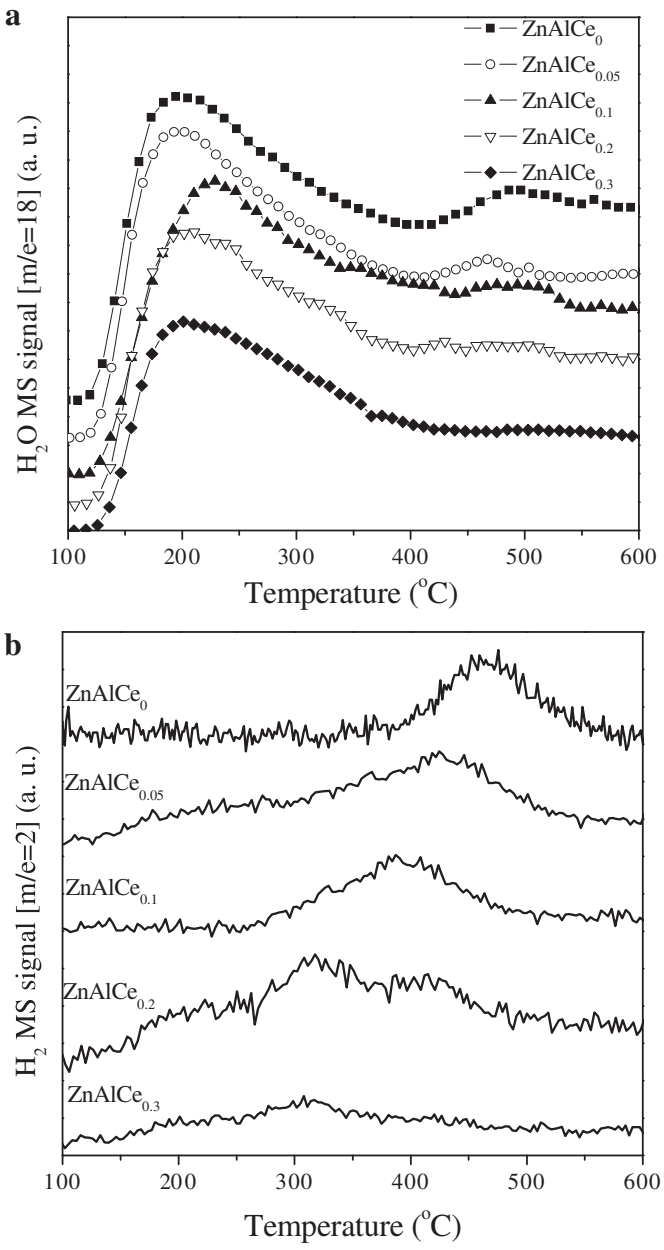

Fig. 8. H_2O-TPD profiles of the $ZnAlCe_x$ catalysts: (a) H_2O signal; (b) H_2 signal.

$$H_2O + A + B \leftrightarrow HO_{(A)} + H_{(B)} \text{ (A: metal ion; B: surface O)} \quad (7)$$

$$2Zn^{2+}\text{–}O(H)\text{–}Zn^{2+} \leftrightarrow 2Zn^{2+}\text{–}O\text{–}Zn^{2+} + H_2 \quad (8)$$

$$CH_3OH + (A) + (B) \leftrightarrow CH_3O_{(A)} + H_{(B)} \text{ (A: metal ion; B: surface O)} \quad (9)$$

3.2.4. CH_3OH pulse adsorption and CH_3OH-TPD

To further understand the interaction between CH_3OH and $ZnAlCe_x$ catalysts, CH_3OH pulse adsorption and CH_3OH-TPD were conducted, the results of which are shown in Table 1 and Fig. 9. Similar to water adsorption on $ZnAlCe_x$, the profile of methanol adsorption may be described as Eq. (9). As the Ce content increases from 5 wt% to 20 wt%, the catalysts exhibit increasing CH_3OH adsorption capacity, suggesting that the doped CeO_2 can strongly interact with methanol; however, as it is further increased from 20 wt % to 30 wt%, the CH_3OH adsorption capacity obviously drops from 0.260 to 0.178 mmol g^{-1}, probably due to the agglomeration of CeO_2 and the decrease of S_{BET} of the sample (from 111 to 80 $m^2\ g^{-1}$). As seen from Fig. 9, the methanol desorption occurs at ~100 °C over all the catalysts. This desorption feature is similar to that on ZnO [24]. Except for CH_3OH, other products such as H_2O, H_2, CO and CO_2 were also monitored. Two H_2O desorption peaks centered at 200–250 °C and 600–700 °C are detected. Considering that the positions of these two desorption peaks are very similar to that of H_2O desorption during H_2O-TPD, the first peak is attributed to the desorption of water molecule formed during methanol adsorption, while the second one may correspond to the water from the interaction of surface −OH groups. With the increase of Ce content, the H_2 desorption peak shifts to lower temperature and gets sharper, which also indicate that the existence of Ce is favorable to the desorption of H_2. It is worth noting that nearly no CO signal is detected for all the catalysts, similar to the CH_3OH-TPD of Au/CeO_2 catalysts [25]. So, it is deduced that the CO formed during DME SR process (as shown in Section 3.1.1) may be produced from other CO-related reactions. In order to further understand the interaction between CH_3OH and catalyst surface, TPSR characterization was also carried out, as elucidated in next section.

3.2.5. TPSR characterization

The TPSR profiles for the co-adsorption of H_2O and CH_3OH on the selected catalysts $ZnAlCe_0$ and $ZnAlCe_{0.2}$ are shown in Fig. 10(a) and (b), respectively. After water adsorption, the CH_3OH pulse adsorption was carried out. It is found that during CH_3OH injection, H_2O can be detected in the effluent gas (not shown), which means that methanol may compete the adsorption sites with water molecule, causing the desorption of some adsorbed H_2O, similar to the situation for H-ZSM-5 [26]. Fig. 10(a) depicts the TPSR results of $ZnAlCe_0$ catalysts. It can be seen that the main desorption products are methanol and water before 219 °C. Further increase of the temperature would cause the simultaneous formation of H_2 and CO_2. When the temperature is increased to 390 °C, no H_2 is detected, instead, H_2O is found in the effluent gas. The TPSR profiles of $ZnAlCe_{0.2}$ are shown in Fig. 10(b). It is found that although the Ce addition to ZnAlO catalyst inhibits the adsorption/desorption of H_2O, the peaks of H_2 and CO_2 get much stronger. Moreover, the temperature for the peaks of H_2 and CO_2 desorption becomes lower (from 330 to 302 °C). These results can be logically correlated with the DME SR activity of Ce-containing catalysts.

3.3. Catalyst stability

The stability of the catalysts is rather important for practical application. So, start-off stability test was performed on the catalyst

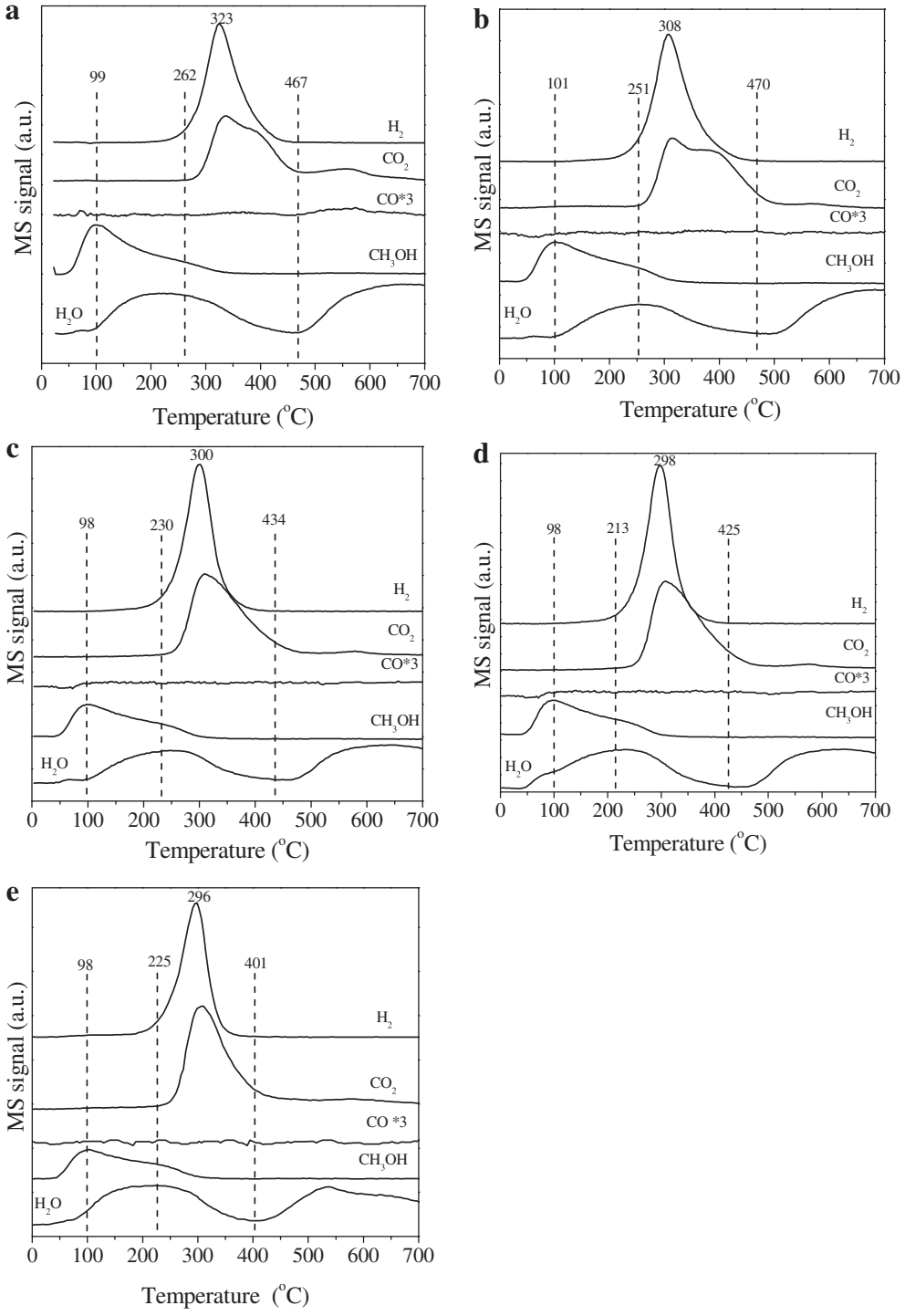

Fig. 9. CH_3OH-TPD profiles of different catalysts: (a) $ZnAlCe_0$; (b) $ZnAlCe_{0.05}$; (c) $ZnAlCe_{0.1}$; (d) $ZnAlCe_{0.2}$; (e) $ZnAlCe_{0.3}$.

$ZnAlCe_{0.2}$, in which 14 h cyclic heating to 420 °C and cooling to RT in the DME SR feed stream was performed. The results shown in Fig. 11 indicate that this catalyst possesses very high stability. During the start-off test, as the temperature is increased to 420 °C the activity is almost recovered to the initial level without obvious change. In a summary, the catalyst $ZnAlCe_{0.2}$ possesses not only high catalytic activity including high DME conversion and high CO_2 selectivity but also high stability, which makes it promising for practical hydrogen production via DME SR.

4. Discussion

4.1. Physicochemical properties, methanol-TPD and reaction mechanism

The mixed $ZnAlCe_x$ and Al_2O_3 has been proved to be highly active for DME SR reaction. The introduction of Ce to ZnAlO oxide decreases the Al content in the catalyst, leading to the decrease of S_{BET}; the larger Ce content, the smaller specific surface area.

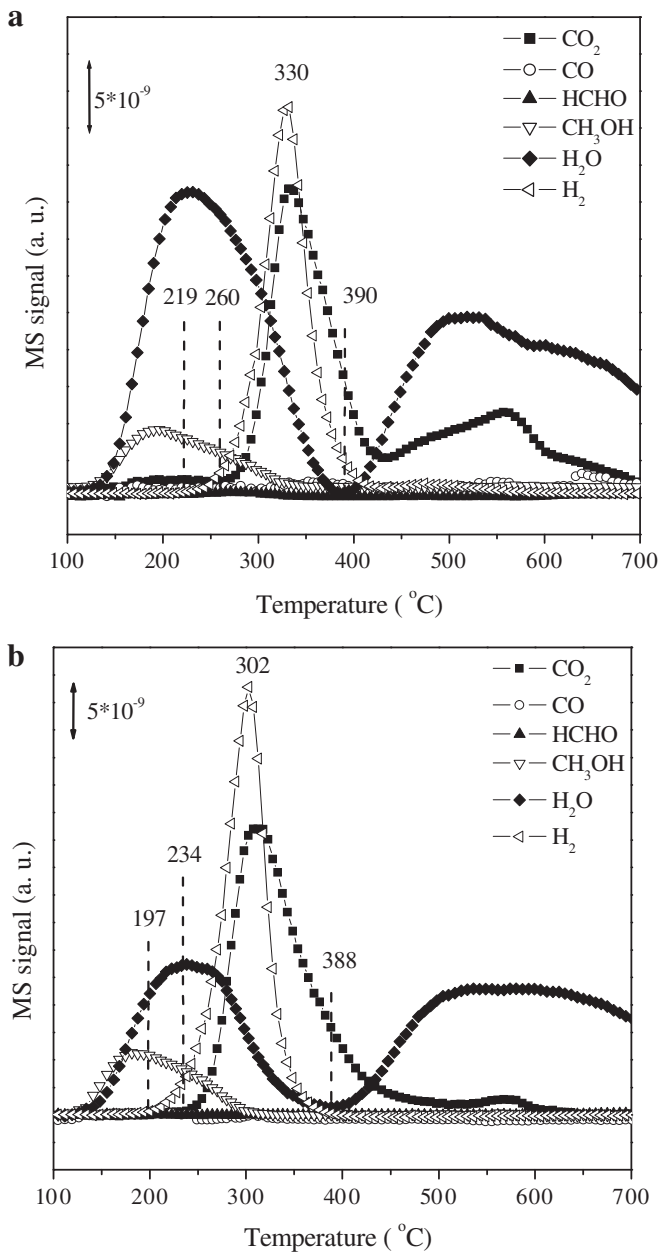

Fig. 10. TPSR profiles of $ZnAlCe_0$ (a) and $ZnAlCe_{0.2}$ (b).

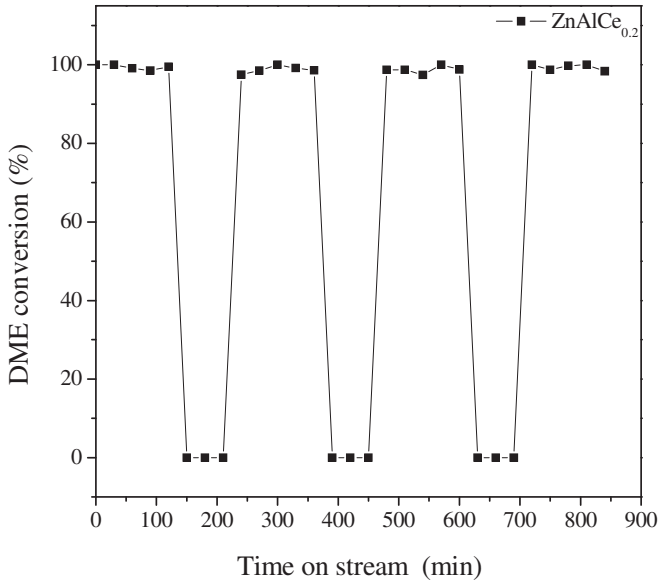

Fig. 11. Stability tests of the $ZnAlCe_{0.2}$ catalyst in cyclic heating to 420 °C and cooling to RT in the DME SR reaction stream for 14 h.

Meanwhile, with the decrease of Al content in the substituted samples the amount of spinel $ZnAl_2O_4$ decreases, making more zinc exist in the form of ZnO as demonstrated by XRD (Fig. 6), XANES (Fig. 7(a)). The existence of Ce also decreases the crystallite size of ZnO and $ZnAl_2O_4$ as elucidated by the results of XRD (Fig. 6) and RSFs from EXAFS (Fig. 7(b)). The promotional effect of Ce on the dispersion of zinc species has also been revealed in CeO_2–ZnO binary oxide systems [27,28]. Between ceria and zinc oxide there may exist interaction. However, no peak shift is observed for ZnO and CeO_2 phases in the XRD patterns (Fig. 6), which suggests that no detectable solid solution or complex oxides are formed. It is known that XRD can only detect the bulk phases, the small amounts of interaction phases at the interface of CeO_2 and ZnO is hard to be detected by XRD. It is proposed that the addition of Ce to ZnO could cause the formation of interstitial $Zn_xCe^{4+}{}_{1-2x}Ce^{3+}{}_{2x}O_2$ solid solution on ZnO matrix [27–29]. In this work, the interstitial $Zn_xCe^{4+}{}_{1-2x}Ce^{3+}{}_{2x}O_2$ solid solution may be also formed at the boundary region due to the substitution of some Ce^{4+} (0.087 nm) by smaller Zn^{2+} (0.074 nm).

During methanol-TPD, the simultaneous release of H_2 and CO_2 rather than H_2 and CO was observed, indicating that the oxidation of methanol on $ZnAlCe_x$ is the major pathway while the direct decomposition of methanol to CO and H_2 is not the dominant one. It is reported that during methanol-TPD over dehydroxylated ZnO (pretreated with pure He at 825 K), only a small CO_2 peak was observed, and the decomposition of methanol to CO and H_2 is the main reaction [24]. However, in this work, the $ZnAlCe_x$ catalysts contain a significant amount of Al_2O_3, which possesses lots of surface −OH groups. According to literature [30], even after vacuum degassing at 400 °C it is hard to remove the −OH groups over Al_2O_3 surface, especially the isolated and some associated hydroxyl groups. Thus, it is believed that there is abundance of surface hydroxyl groups on $ZnAlCe_x$ catalysts before methanol adsorption. When the pulse of methanol was introduced to the catalyst bed, methanol could be dissociatively adsorbed on the active site. With the increase of the temperature of catalyst bed, the adsorbed methanol may react with hydroxyl groups to form CO_2 and H_2, as shown in Eq. (10).

$$CH_3OH + -OH_{(A)} \rightarrow CO_2 + \frac{5}{2}H_2 + A \quad (10)$$

The MSR mechanisms on Cu-based catalysts have been extensively investigated and discussed in literature [31,32]. It is assumed that two kinds of active sites are necessary for MSR reaction, the active site A (metal ions) is responsible for the adsorption of oxygen-containing intermediates such as CH_3O and the active site B (lattice oxygen ions) is responsible for hydrogen extraction from the above-mentioned intermediates [31]. It is know that the key steps of methanol synthesis reaction are the H_2 dissociative adsorption on Cu particles, and the following transfer of atomic H to the oxide surface by spillover [23]. So, the MSR reaction on Cu-based catalysts may be accomplished by the spillover of atomic H onto the Cu sites and the subsequent formation of H_2 through the combination of atomic H. As to the MSR reaction mechanism over Zn-based catalysts, the Zn^{2+}–O–Zn^{2+} linkages should be

responsible for H_2 formation based on the H_2O-TPD results. The reaction mechanism of MSR over Zn-based catalysts could be described as Eqs. (7)–(14) and Scheme 1. Methanol generated by DME hydrolysis may be adsorbed dissociatively onto the active site A and B, then the $CH_3O_{(A)}$ species dehydrogenate to form adsorbed HCHO, followed by a nucleophilic attack of H_2O to produce adsorbed HCOOH, which can decompose to H_2 and CO_2. The TPSR results (Fig. 10) have demonstrated that H_2 and CO_2 always desorb simultaneously, indicating that the intermediate formed by methanol dehydrogenation should react quickly to generate H_2 and CO_2; as a result, their desorption temperatures are always close to each other. Based upon the above discussion, the methanol dehydrogenation (Eq. (11)) is believed to be the rate-determining step (RDS), similar to the situation for MSR reaction over Cu-based catalysts reported in literature [32].

$$CH_3O_{(A)} + H_{(B)} \leftrightarrow CH_2O_{(A)} + H_2 + (B) \quad (11)$$

$$CH_2O_{(A)} + HO_{(A)} + (B) \leftrightarrow HCOOH_{(A)} + H_{(B)} + (A) \quad (12)$$

$$H_{(B)} + H_{(B)} \leftrightarrow H_2 + 2(B) \quad (13)$$

$$HCOOH_{(A)} \leftrightarrow CO_2 + H_2 + (A) \quad (14)$$

4.2. Activity and selectivity correlation

The activity results (Fig. 1) have shown that over Ce-substituted samples the DME conversion is increased with Ce content increasing up to 20 wt%. It is found that during H_2O-TPD the H_2 desorption temperature is decreased with Ce content increasing up to 20 wt%. In addition, the H_2 desorption peak for Ce-containing catalysts is sharper as seen in CH_3OH-TPD profiles (Fig. 9). The function of Ce may be related to the capability of Ce–O bonds for the production of $H^{\delta-}$ and $H^{\delta+}$ species [23,33]. With the increase of Ce content, the CO_2 desorption peaks shift to lower temperatures, indicating that the addition of Ce also facilitates the desorption of CO_2. According to the reaction mechanism, the active site A is occupied by the oxygen-containing species such as CH_3O, HCOOH and CO_2. The desorption of CO_2 could release the active site A, enhancing the re-adsorption of methanol on the active site and thus promoting the reaction. On the basis of these results, it is deduced that the higher activity of Ce-substituted catalysts could be attributed to their better H_2 desorption capability and better CO_2 desorption capability. According to the discussion of physicochemical properties, the introduction of Ce into ZnAlO may facilitate the formation of interstitial $Zn_xCe^{4+}{}_{1-2x}Ce^{3+}{}_{2x}O_2$ solid solution at the boundary of CeO_2 and Zn species. The formed interstitial $Zn_xCe^{4+}{}_{1-2x}Ce^{3+}{}_{2x}O_2$ solid solution contains abundance of Ce^{4+}–O–Zn^{2+} linkages. As discussed in the reaction mechanism, hydrogen extraction from methanol or other intermediates is conducted on the lattice oxygen ions, such as the oxygen in Zn^{2+}–O–Zn^{2+} linkage of the $ZnAlCe_0$ catalyst and in the Ce^{4+}–O–Zn^{2+} linkage of the Ce-containing catalysts. During MSR process, the Ce^{4+}–O–Zn^{2+} linkage is believed to be more active than the Zn^{2+}–O–Zn^{2+} linkage for the extraction of H atom from CH_3OH molecule to form Ce^{4+}–O(H)–Zn^{2+} or Zn^{2+}–O(H)–Zn^{2+} species. It means that the presence of Ce may improve the MSR activity by enhancing the rate-determining step. Higher Ce content than 20 wt% would bring a detrimental influence on the adsorption of H_2O and methanol (Table 1) due to the significant decrease of specific surface area (from 111 to 80 $m^2\ g^{-1}$). Through calculation, it is found that with Ce content increasing from 0 to 30 wt%, the TOF increases from 0.013 to 0.035 s^{-1}. This is consistent with the CH_3OH-TPD results, which indicate that the H_2 desorption temperature decreases from 323 to 296 °C with Ce content increasing from 0 to 30 wt%. The apparent activation energy Ea (Table 1) of the $ZnAlCe_x$ catalysts for DME SR is in the range of 184.1–195.5 kJ mol^{-1}, which is a little higher than that (150–160 kJ mol^{-1}) for Cu-based catalysts [18,33]. For MSR over Zn-based catalyst, much higher apparent activation energy (~144 kJ mol^{-1}) was also found [14], as compared with that (76.9–85.7 kJ mol^{-1}) for Cu-based catalyst [31]. In this work, the presence of 20% Ce in $ZnAlCe_x$ catalysts can decrease the activation energy from 195.5 kJ mol^{-1} to 184.1 kJ mol^{-1}, suggesting the alteration of active sites or reaction pathways, e.g., the appearance of Ce^{4+}–O–Zn^{2+} linkages. In a summary, the introduction of Ce (≤20 wt%) to ZnAlO catalysts can facilitate the dehydrogenation of methanol, decreasing the activation energy and increasing the TOF of DME SR; as a result, the catalytic activity including DME conversion and H_2 yield is improved.

From CO/CO_2 selectivity profiles displayed in Fig. 4(a) and (b), we can see that the CO_2 selectivity is much higher than that for the byproduct CO. It is reported that DME SR reaction over Cu-based catalysts is accomplished by MSR reaction, followed by the r-WGS reaction, which is the main source of CO [7,34]. In this work, the CO concentrations in the products are much lower than the equilibrium concentration. Thus, CO may be not formed through methanol decomposition, probably via the r-WGS reaction. This deduction is strongly supported by the TPSR results, in which nearly no CO was detected in the effluent gas. After Ce addition CO selectivity is lowered but CO_2 selectivity is increased, indicating the enhanced formation of CO_2 rather than CO, which is also evidenced by the results of CH_3OH-TPD (Fig. 9), namely, the desorption peak of CO_2 becomes sharper when Ce is doped into the Zn-based catalyst. The Ce addition is favorable to the redox property of the catalysts, which accounts for the enhanced CO_2 formation during DME SR [17].

5. Conclusion

The as-prepared mixed oxide catalysts $ZnAlCe_x$ with Al partially substituted by Ce possess rather high catalytic activity for DME SR

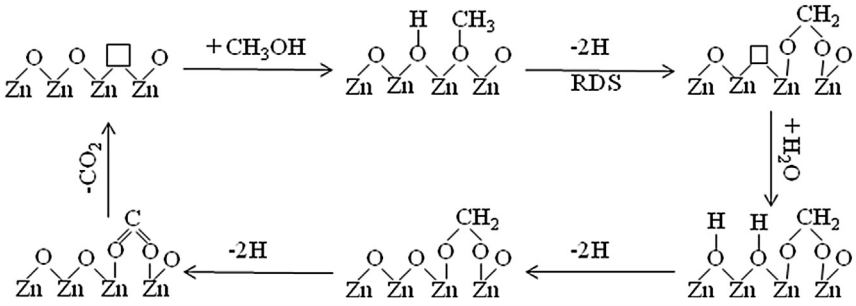

Scheme 1.

to produce H_2. The DME conversion, H_2 yield, CO selectivity and the stability of the $ZnAlCe_x$ catalysts are largely dependent on Ce content. The optimized content of Ce in $ZnAlCe_x$ is 20 wt%. XRD and EXAFS results reveal that the introduction of Ce to ZnAlO oxide not only inhibits the transformation of ZnO to spinel $ZnAl_2O_4$, but also enhances the dispersion of Zn species. H_2O-TPD and CH_3OH-TPD results reveal that the partial substitution of Al by Ce can facilitate the generation of H_2 and CO_2, which is highly related to the better catalytic performance of Ce-containing catalysts for DME SR. The methanol dehydrogenation is identified to be the rate-determining step of MSR over Zn-based catalysts. The decrease of apparent activation energy (E_a) induced by the Ce addition suggests the formation of new reaction sites such as the Ce^{4+}–O–Zn^{2+} linkages at the oxides interface.

Acknowledgments

This work is financially supported by the National Natural Science Foundation of China (Nos. 21276184, U1332102, 21276187), the Specialized Research Fund for the Doctoral Program of Higher Education of China (No. 20120032110014), the Program for Introducing Talents of Discipline to Universities of China (No. B06006) and the Engineering Education Funding of Tianjin University.

References

[1] D.E. Curtin, R.D. Lousenberg, T.J. Henry, P.C. Tangeman, M.E. Tisack, J. Power Sources 131 (2004) 41–48.
[2] J. Zhang, Z. Xie, J. Zhang, Y. Tang, C. Song, T. Navessin, Z. Shi, D. Song, H. Wang, D.P. Wilkinson, Z.-S. Liu, S. Holdcroft, J. Power Sources 160 (2006) 872–891.
[3] A.S.P. Lovón, J.J. Lovón-Quintana, G.I. Almerindo, G.P. Valença, M.I.B. Bernardi, V.D. Araújo, T.S. Rodrigues, P.A. Robles-Dutenhefner, H.V. Fajardo, J. Power Sources 216 (2012) 281–289.
[4] L. Pérez-Moreno, J. Soler, J. Herguido, M. Menéndez, J. Power Sources 243 (2013) 233–241.
[5] S.G. Sanches, J.H. Flores, R.R. de Avillez, M.I. Pais da Silva, Int. J. Hydrogen Energy 37 (2012) 6572–6579.
[6] S.D. Badmaev, P.V. Snytnikov, Int. J. Hydrogen Energy 32 (2008) 3026–3030.
[7] Z. Sun, M. Meng, L. Zhang, Y. Zha, X. Zhou, Z. Jiang, S. Zhang, Y. Huang, Int. J. Hydrogen Energy 37 (2012) 18860–18869.
[8] X. Zhou, M. Meng, Z. Sun, Q. Li, Z. Jiang, Chem. Eng. J. 174 (2011) 400–407.
[9] T.A. Semelsberger, K.C. Ott, R.L. Borup, H.L. Greene, Appl. Catal. B 65 (2006) 291–300.
[10] N. Shimoda, K. Faungnawakij, R. Kikuchi, K. Eguchi, Int. J. Hydrogen Energy 36 (2011) 1433–1441.
[11] T.A. Semelsberger, K.C. Ott, R.L. Borup, H.L. Greene, Appl. Catal. B 61 (2005) 281–287.
[12] I. Sierra, J. Ereña, A.T. Aguayo, J.M. Arandes, J. Bilbao, Appl. Catal. B 94 (2010) 108–116.
[13] D. Feng, Y. Wang, D. Wang, J. Wang, Chem. Eng. J. 146 (2009) 477–485.
[14] H. Lorenz, M. Friedrich, M. Armbrüster, B. Klötzer, S. Penner, J. Catal. 297 (2013) 151–154.
[15] M. Yang, S. Li, G. Chen, Appl. Catal. B 101 (2011) 409–416.
[16] M. Yang, Y. Men, S. Li, G. Chen, Int. J. Hydrogen Energy 37 (2012) 8360–8369.
[17] P. Fornasiero, G. Balducci, R.D. Monte, J. Kašpar, V. Sergo, G. Gubitosa, A. Ferrero, M. Graziani, J. Catal. 164 (1996) 173–183.
[18] L. Zhang, M. Meng, S. Zhou, Z. Sun, J. Zhang, Y. Xie, T. Hu, J. Power Sources 232 (2013) 286–296.
[19] R. Kam, C. Selomulya, R. Amal, J. Scott, J. Catal. 273 (2010) 73–81.
[20] S. Pin, M. Suardelli, F. D'Acapito, G. Spinolo, M. Zema, S.C. Tarantino, P. Ghigna, J. Phys. Chem. C 117 (2013) 6105–6112.
[21] A. Önsten, D. Stoltz, P. Palmgren, S. Yu, M. Göthelid, U.O. Karlsson, J. Phys. Chem. C 114 (2010) 11157–11161.
[22] M. Fronzi, S. Piccinin, B. Delley, E. Traversa, C. Stampfl, Phys. Chem. Chem. Phys. 11 (2009) 9188–9199.
[23] K.A. Pokrovski, A.T. Bell, J. Catal. 241 (2006) 276–286.
[24] D. Chadwick, K. Zheng, Catal. Lett. 20 (1993) 231–242.
[25] N. Yi, R. Si, H. Saltsburg, M. Flytzani-Stephanopoulos, Energy Environ. Sci. 3 (2010) 831–837.
[26] A. Ison, R.J. Gorte, J. Catal. 89 (1984) 150–158.
[27] B.G. Mishra, G.R. Rao, Bull. Mater. Sci. 25 (2002) 155–162.
[28] B.G. Mishra, G.R. Rao, J. Mol. Catal. A Chem. 243 (2006) 204–213.
[29] R. Li, S. Yabe, M. Yamashita, S. Momose, S. Yoshida, S. Yin, T. Sato, Solid State Ionics 115 (2002) 235–241.
[30] T.H. Ballinger, J.T. Yates Jr., Langmuir 7 (1991) 3041–3045.
[31] B. Frank, F.C. Jentoft, H. Soerijanto, J. Kröhnert, R. Schlögl, R. Schomäcker, J. Catal. 246 (2007) 177–192.
[32] S. Sá, H. Silva, L. Brandão, J.M. Sousa, A. Mendes, Appl. Catal. B 99 (2010) 43–57.
[33] C. Lamonier, A. Ponchel, A. D'huysser, L. Jalowiecki-Duhamel, Catal. Today 20 (1999) 247–259.
[34] K. Faungnawakij, T. Fukunaga, R. Kikuchi, K. Eguchi, J. Catal. 256 (2008) 37–44.